

# An Approach from Lattice Computing to fMRI Analysis

Manuel Graña, Maite García-Sebastián, Ivan Villaverde, Elsa Fernandez

Grupo de Inteligencia Computacional, UPV/EHU  
[www.ehu.es/ccwitnco](http://www.ehu.es/ccwitnco)

**Abstract.** We introduce an approach to fMRI analysis based on the Lattice Associative Memory (LAM) Endmember Induction Heuristic Algorithm (EIHA). Induced endmembers are used to compute the activation levels of voxels as result of an unmixing process. The endmembers correspond to diverse activation patterns, one of these activation patterns corresponds to the rest state of the neuronal tissue. We introduce a lattice normalization which consists in the mean centering for each voxel pattern independently. This lattice normalization is needed to remove scaling effects that rendered our approach inapplicable. Results on a case study are encouraging.

## 1 Introduction

Human brain mapping is a rapidly expanding discipline, and in recent years interest has grown in novel methods for imaging human brain functionality. Noninvasive techniques can measure cerebral physiologic responses during neural activation. One of the relevant techniques is functional magnetic resonance imaging (fMRI) [6], which uses the blood oxygenation level dependent (BOLD) contrast. Slight physiological alterations, such as neuronal activation resulting in changes of blood flow and blood oxygenation, are detected. These signal changes are related to changes in the concentration of deoxy-hemoglobin, which acts as an intravascular contrast agent for fMRI. The most fMRI examinations are performed with BOLD-based methods using techniques sensitive to local distortions in the magnetic field (susceptibility sensitive techniques). These are T2 weighted spin echo pulse sequences or T2\* weighted gradient echo pulse sequences. The various fMRI-methods have a good spatial and temporal resolution, limited only by the precision with which the autoregulatory mechanisms of the brain adjust blood flow in space to the metabolic demands of neuronal activity. Since these methods are completely noninvasive, using no contrast agent or ionizing radiation, repeated single-subject studies are becoming feasible [5].

To evaluate the resulting fMRI image series, sophisticated algorithms and great computational power are needed to separate the physiologically induced signals from noise or from artifacts resulting from patient movement or MRI detection techniques [13]. Appropriate postprocessing procedures for fMRI are currently being developed at a very rapid pace. Since many research groups are working in this area, no consensus has been reached about the analysis methods of the functional data up to now. A further reason for the large variety of different postprocessing procedures is the lack of a complete underlying theory of the BOLD effect.

The fMRI experiment consists of a functional template or protocol (e.g., alternating activation and rest for a certain time) that induces a functional response in the brain. The aim of an fMRI experiment is to detect this stimulus response, resulting from the BOLD effect, in a defined volume element (voxel). The functional information of a voxel has to be extracted from its functional time course. Therefore, for each functional time point one fMRI volume is recorded. The complete four-dimensional dataset (three dimensions in space, one dimension in time) consists of subsequently recorded three-dimensional (3-D) volumes and thus for each voxel of a volume a functional time course exists. The acquisition of these functional volumes runs over periods lasting up to several minutes.

There are a number of sources of noise in the fMRI signal [14] that must be dealt with in appropriate preprocessing steps. The pulse sequence and the magnetic field strength used can have an effect on the image quality. The long time duration of the experiments allow for head motions, even with strong restriction put into place. Experiment designs also affect the relative dynamics. We will assume that these noise sources have been dealt with appropriately.

The most extended analysis approach for fMRI signals is the Statistical Parametric Maps (SPM) [2] which has developed into a free open source software package. This method consists in the separate voxel based test of the generalized linear model (GLM) corresponding to the experimental design, followed by a segmentation of the spatial distribution of the individual voxel t-test values as a parametric map. There have been also approximations based on the Independent Component Analysis (ICA) [1] assuming that the time series observations are linear mixtures of independent sources which can not be observed. ICA assumes that the source signals are non-Gaussian and that the linear mixing process is unknown. The approaches to solve the ICA process obtain both the independent sources and the linear unmixing matrix. In previous works we have proposed an heuristic algorithm, which we have called Endmember Induction Heuristic Algorithm (EIHA) in [3] to solve a similar problem. There the assumption is that the data is generated from a set of endmembers which are the vertices of a convex polytope covering the data observations. Our approach is based on the relation between the Lattice Independence and Affine Independence [12], and the ability of Lattice Associative Memories to serve as detectors of Lattice Independent sets of vectors. The original works were devoted to unsupervised hyperspectral image segmentation, and here we try to apply it to fMRI analysis. The results are promising. This approach falls in the field of Lattice Computing algorithms, which have been introduced in [4] as the class of algorithms that either apply lattice operators inf and sup or use lattice theory to produce generalizations or fusions of previous approaches. In [4] an extensive and updated list of references, including previous works from authors contributing to this workshop, can be found.

The outline of the paper is as follows: Section 2 will present the underlying linear mixing model. Section 3 presents an sketch of the relation between Lattice Independence and Linear (Affine) Independence through the LAM theory. Section 4 recalls our heuristic algorithm. Section 5 presents results of the proposed approach on a case study. Section 6 provides some conclusions.

## 2 The Linear Mixing Model

The linear mixing model can be expressed as follows:

$$\mathbf{x} = \sum_{i=1}^M a_i \mathbf{s}_i + \mathbf{w} = \mathbf{S}\mathbf{a} + \mathbf{w}, \quad (1)$$

where  $\mathbf{x}$  is the  $d$ -dimension pattern vector corresponding to the fMRI voxel time series vector,  $\mathbf{S}$  is the  $d \times M$  matrix whose columns are the  $d$ -dimension vertices of the convex region covering the data corresponding to the so called endmembers  $\mathbf{s}_i, i = 1, \dots, M$ ,  $\mathbf{a}$  is the  $M$ -dimension fractional abundance vector, and  $\mathbf{w}$  is the  $d$ -dimension additive observation noise vector. The linear mixing model is subjected to two constraints on the abundance coefficients. First, to be physically meaningful, all abundance coefficients must be non-negative  $a_i \geq 0, i = 1, \dots, M$ . Second, to account for the entire composition, they must be fully additive  $\sum_{i=1}^M a_i = 1$ . That means that we expect the vectors in  $\mathbf{S}$  to be affinely independent and that the convex region defined by them includes *all* the data points.

Once the convex region vertices have been determined the unmixing process is the computation of the matrix inversion that gives the coordinates of the point relative to the convex region vertices. The simplest approach is the unconstrained least squared error (LSE) estimation given by:

$$\hat{\mathbf{a}} = (\mathbf{S}^T \mathbf{S})^{-1} \mathbf{S}^T \mathbf{x}. \quad (2)$$

The coefficients that result from equation 2 do not necessarily fulfill the non-negativity and full additivity conditions. For simplicity, we will use the unconstrained estimation of equation 2 to compute the abundance coefficients. Moreover, the heuristic algorithm EIHA described in section 4 from [3] always produces convex regions that lie inside the data cloud, so that enforcing the non-negative and additivity to one conditions would be impossible for some data points. Negative values are considered as zero values and the additivity to one condition is not important as long as we are looking for the maximum abundances to assign meaning to the resulting spatial distribution of the coefficients. These coefficients are interpreted as fMRI voxel activation. That is, high positive values are interpreted as high voxel activation if the corresponding endmember does not correspond to the random pattern obtained as the resting state response.

## 3 Lattice Independence and Lattice Autoassociative Memories

The work on Lattice Associative Memories (LAM) stems from the consideration of the algebraic lattice structure  $(\mathbb{R}, \vee, \wedge, +)$  as the alternative to the algebraic framework given by the mathematical field  $(\mathbb{R}, +, \cdot)$  for the definition of Neural Networks computation. The LAM were first introduced in [8,9] as Morphological Associative Memories, but we follow the new convention introduced in [11,12] because it sets the works in the more general framework of Lattice Computing. The operators  $\vee$  and  $\wedge$  denote, respectively, the discrete max and min operators (resp. sup and inf in a continuous setting).

Given a set of input/output pairs of pattern  $(X, Y) = \{(\mathbf{x}^\xi, \mathbf{y}^\xi); \xi = 1, \dots, k\}$ , a linear heteroassociative neural network based on the pattern's cross correlation is built up as  $W = \sum_{\xi} \mathbf{y}^\xi \cdot (\mathbf{x}^\xi)'$ . Mimicking this constructive procedure [8,9] propose the following constructions of Lattice Memories (LM):

$$W_{XY} = \bigwedge_{\xi=1}^k [\mathbf{y}^\xi \times (-\mathbf{x}^\xi)'] \text{ and } M_{XY} = \bigvee_{\xi=1}^k [\mathbf{y}^\xi \times (-\mathbf{x}^\xi)'], \quad (3)$$

where  $\times$  is any of the  $\boxtimes$  or  $\boxminus$  operators. Here  $\boxtimes$  and  $\boxminus$  denote the max and min matrix product [8,9]. respectively defined as follows:

$$C = A \boxtimes B = [c_{ij}] \Leftrightarrow c_{ij} = \bigvee_{k=1, \dots, n} \{a_{ik} + b_{kj}\}, \quad (4)$$

$$C = A \boxminus B = [c_{ij}] \Leftrightarrow c_{ij} = \bigwedge_{k=1, \dots, n} \{a_{ik} + b_{kj}\}. \quad (5)$$

If  $X = Y$  then the LM memories are Lattice Autoassociative Memories (LAM). Conditions of perfect recall by the LM and LAM of the stored patterns proved in [8,9] encouraged the research on them, because in the continuous case, the LAM is able to store and recall any set of patterns:  $W_{XX} \boxtimes X = X = M_{XX} \boxminus X$ , for any  $X$ . However, this result holds when we deal with noise-free patterns. Research on robust recall [7,9,10] based on the so-called kernel patterns lead to the notion of morphological independence, in the erosive and dilative sense, and finally to the definition of Lattice Independence (LI) and Strong Lattice Independence (SLI). We gather some results from [12] that set the theoretical background for the approach to endmember induction applied.

**Definition 1.** Given a set of vectors  $\{\mathbf{x}^1, \dots, \mathbf{x}^k\} \subset \mathbb{R}^n$  a linear minimax combination of vectors from this set is any vector  $\mathbf{x} \in \mathbb{R}_{\pm\infty}^n$  which is a linear minimax sum of these vectors:

$$x = \mathcal{L}(\mathbf{x}^1, \dots, \mathbf{x}^k) = \bigvee_{j \in J} \bigwedge_{\xi=1}^k (a_{\xi j} + \mathbf{x}^\xi),$$

where  $J$  is a finite set of indices and  $a_{\xi j} \in \mathbb{R}_{\pm\infty} \forall j \in J$  and  $\forall \xi = 1, \dots, k$ .

**Definition 2.** The linear minimax span of vectors  $\{\mathbf{x}^1, \dots, \mathbf{x}^k\} = X \subset \mathbb{R}^n$  is the set of all linear minimax sums of subsets of  $X$ , denoted  $LMS(\mathbf{x}^1, \dots, \mathbf{x}^k)$ .

**Definition 3.** Given a set of vectors  $X = \{\mathbf{x}^1, \dots, \mathbf{x}^k\} \subset \mathbb{R}^n$ , a vector  $\mathbf{x} \in \mathbb{R}_{\pm\infty}^n$  is lattice dependent if and only if  $x \in LMS(\mathbf{x}^1, \dots, \mathbf{x}^k)$ . The vector  $\mathbf{x}$  is lattice independent if and only if it is not lattice dependent on  $X$ . The set  $X$  is said to be lattice independent if and only if  $\forall \lambda \in \{1, \dots, k\}$ ,  $\mathbf{x}^\lambda$  is lattice independent of  $X \setminus \{\mathbf{x}^\lambda\} = \{\mathbf{x}^\xi \in X : \xi \neq \lambda\}$ .

The definition of lattice independence supersedes and improves the early definitions [10] of erosive and dilative morphological independence, which, however, have more intuitive appealing. Nevertheless, this definition has the additional advantage of establishing a formal parallelism with the definition of linear independence.

**Definition 4.** A set of vectors  $X = \{\mathbf{x}^1, \dots, \mathbf{x}^k\} \subset \mathbb{R}^n$  is said to be max dominant if and only if for every  $\lambda \in \{1, \dots, k\}$  there exists an index  $j_\lambda \in \{1, \dots, n\}$  such that

$$x_{j_\lambda}^\lambda - x_i^\lambda = \bigvee_{\xi=1}^k (x_{j_\lambda}^\xi - x_i^\xi) \quad \forall i \in \{1, \dots, n\}.$$

Similarly,  $X$  is said to be min dominant if and only if for every  $\lambda \in \{1, \dots, k\}$  there exists an index  $j_\lambda \in \{1, \dots, n\}$  such that

$$x_{j_\lambda}^\lambda - x_i^\lambda = \bigwedge_{\xi=1}^k (x_{j_\lambda}^\xi - x_i^\xi) \quad \forall i \in \{1, \dots, n\}.$$

The expressions that compound this definition appeared in the early theorems about perfect recall of Morphological Associative Memories [8,9]. Their value as an identifiable property of the data has been discovered in the context of the formalization of the relationship between strong lattice independence, defined below, and the classical affine independence.

**Definition 5.** A set of lattice independent vectors  $\{\mathbf{x}^1, \dots, \mathbf{x}^k\} \subset \mathbb{R}^n$  is said to be strongly lattice independent (SLI) if and only if  $X$  is max dominant or min dominant or both.

As said before, min and max dominance are the conditions for perfect recall. Per construction, the column vectors of Lattice Autoassociative Memories are min or max dominant, depending of their erosive or dilative nature, therefore they will be strongly lattice independent, if they are lattice independent.

*Conjecture 1.* [12] If  $X = \{\mathbf{x}^1, \dots, \mathbf{x}^k\} \subset \mathbb{R}^n$  is strongly lattice independent then  $X$  is affinely independent.

This conjecture (stated as theorem in [11]) is the key result whose proof would relate the linear convex analysis and the non-linear lattice analysis. If true, it means that the construction of the LAM provides the starting point for obtaining sets of affine independent vectors that could be used as endmembers for the unmixing algorithms described in section 2.

**Theorem 1.** [12] Let  $X = \{\mathbf{x}^1, \dots, \mathbf{x}^k\} \subset \mathbb{R}^n$  and let  $W$  ( $M$ ) be the set of vectors consisting of the columns of the matrix  $W_{XX}$  ( $M_{XX}$ ). Let  $F(X)$  denote the set of fixed points of the LAM constructed from set  $X$ . There exist  $V \subset W$  and  $N \subset M$  such that  $V$  and  $N$  are strongly lattice independent and  $F(X) = F(V) = F(N)$  or, equivalently,  $W_{XX} = W_{VV}$  and  $M_{XX} = M_{NN}$ .

The key idea of this theorem is to test the lattice independence of the already known as min or max dominant sets of vectors. Removing lattice dependent vectors will not affect this min/max dominance property. The smart way to test lattice dependence lies in the fact that removing a lattice dependent vectors does not alter the set of fixed points of the remaining ones. This theorem is proved following a constructive reasoning, giving way to an algorithm for the construction of the set of affine independent sets of vectors from LAM discussed in [3,12].

**Algorithm 1** Endmember Induction Heuristic Algorithm (EIHA)

- 
1. Shift the data sample to zero mean  
 $\{\mathbf{f}^c(i) = \mathbf{f}(i) - \vec{\mu}; i = 1, \dots, n\}$ .
  2. Initialize the set of vertices  $E = \{\mathbf{e}_1\}$  with a randomly picked sample. Initialize the set of lattice independent binary signatures  $X = \{\mathbf{x}_1\} = \{(e_k^1 > 0; k = 1, \dots, d)\}$
  3. Construct the LAM's based on the lattice independent binary signatures:  $M_{XX}$  and  $W_{XX}$ .
  4. For each pixel  $\mathbf{f}^c(i)$ 
    - (a) compute the noise corrections sign vectors  $\mathbf{f}^+(i) = (\mathbf{f}^c(i) + \alpha \vec{\sigma} > \mathbf{0})$  and  $\mathbf{f}^-(i) = (\mathbf{f}^c(i) - \alpha \vec{\sigma} > \mathbf{0})$
    - (b) compute  $y^+ = M_{XX} \boxtimes \mathbf{f}^+(i)$
    - (c) compute  $y^- = W_{XX} \boxtimes \mathbf{f}^-(i)$
    - (d) if  $y^+ \notin X$  or  $y^- \notin X$  then  $\mathbf{f}^c(i)$  is a new vertex to be added to  $E$ , execute once 3 with the new  $E$  and resume the exploration of the data sample.
    - (e) if  $y^+ \in X$  and  $\mathbf{f}^c(i) > \mathbf{e}_{y^+}$  the pixel spectral signature is more extreme than the stored vertex, then substitute  $\mathbf{e}_{y^+}$  with  $\mathbf{f}^c(i)$ .
    - (f) if  $y^- \in X$  and  $\mathbf{f}^c(i) < \mathbf{e}_{y^-}$  the new data point is more extreme than the stored vertex, then substitute  $\mathbf{e}_{y^-}$  with  $\mathbf{f}^c(i)$ .
  5. The final set of endmembers is the set of original data vectors  $\mathbf{f}(i)$  corresponding to the sign vectors selected as members of  $E$ .
- 

**4 Endmember Induction Heuristic Algorithm (EIHA)**

For the sake of completeness we recall here our Endmember Induction Heuristic Algorithm (EIHA) maintaining the notation used in the original references. Let us denote  $\{\mathbf{f}(i) \in \mathbb{R}^d; i = 1, \dots, n\}$  the high dimensional data that may be the time series in a fMRI voxels,  $\vec{\mu}$  and  $\vec{\sigma}$  are, respectively, the mean vector and the vector of standard deviations computed over the data sample,  $\alpha$  the noise correction factor and  $E$  the set of already discovered vertices. The noise amplitude of the additive noise in equation (1) is  $\vec{\sigma}$ , the patterns are corrected by the addition and subtraction of  $\alpha \vec{\sigma}$ , before being presented to the LAM's. The gain parameter  $\alpha$  controls the amount of flexibility in the discovering of new endmembers. Let us denote by the expression  $\mathbf{x} > \mathbf{0}$  the construction of the binary vector  $(\{b_i = 1 \text{ if } x_i > 0; b_i = 0 \text{ if } x_i \leq 0\}; i = 1, \dots, n)$ . The detailed description of the steps in the heuristic algorithm is presented as Algorithm 1. The starting endmember set consists of a randomly picked pixel. However, this selection is not definitive, because the algorithm may later change this endmember for another, more extreme, one. The noise correction parameter  $\alpha$  has a great impact on the number of endmembers found. Low values imply large number of endmembers. It determines if a vector is interpreted as a random perturbation of an already selected endmember.

**5 A Case Study**

The experimental data corresponds to auditory stimulation test data of single person. It is freely available from <ftp://ftp.fil.ion.ucl.ac.uk/spm/data>, the file name is snrfM00223.zip. These data are the result of the preprocessing pipeline that removes many noise sources.

These whole brain BOLD/EPI images were acquired on a modified 2T Siemens MAGNETOM Vision system. Each acquisition consisted of 64 contiguous slices. Each slice being a 2D image of one head volume cut. There are  $64 \times 64 \times 64$  voxels of size 3mm x 3mm x 3mm. The data acquisition took 6.05s, with the scan-to-scan repeat time (RT) set arbitrarily to 7s. 96 acquisitions were made (RT=7s) in blocks of 6, i.e., 16 42s blocks. The condition for successive blocks alternated between rest and auditory stimulation, starting with rest. Auditory stimulation was bi-syllabic words presented binaurally at a rate of 60 per minute. The functional data starts at acquisition 4, image snrfMOO223-004. Due to T1 effects it is advisable to discard the first few scans (there were no "dummy" lead-in scans). We have discarded the first 10 scans. Figure 1 shows the plots of the time series corresponding to the slice #30 of the collected volume. It can be appreciated that there are an intensity displacement filling the whole range of intensities. There are few voxels showing an activation pattern on the top of the plots, and the vast majority of the voxels time series correspond to random non activation patterns at diverse intensities. The result of our algorithm applied to these raw data would be trivial and uninteresting, we would find the upper and lower patterns.

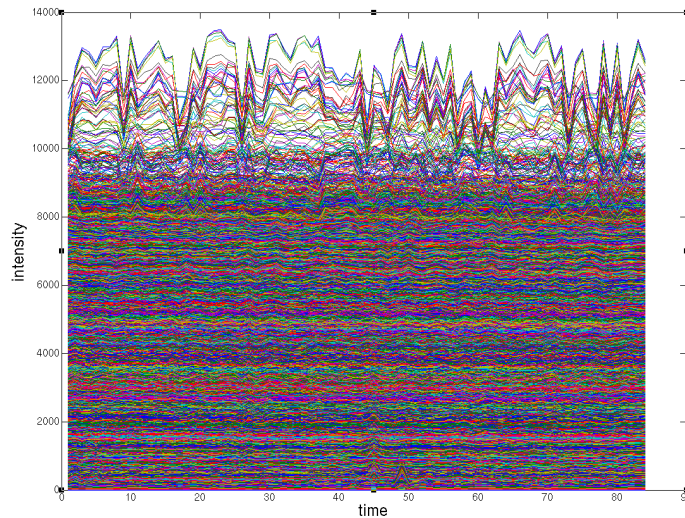


**Fig. 1.** Plot of the time series for the voxels of axial slice #30.

After subtracting its mean to each voxel time series independently, the plots are collapsed as shown in figure 2 around the origin. It can be appreciated that most deactivated voxels are collapsed into a quite similar pattern, and that the diverse activation patterns stand out. This mean subtraction corresponds to a scale normalization in the lattice computing sense. It removes scale effects that hinder the detection of meaningful lattice independent vectors.

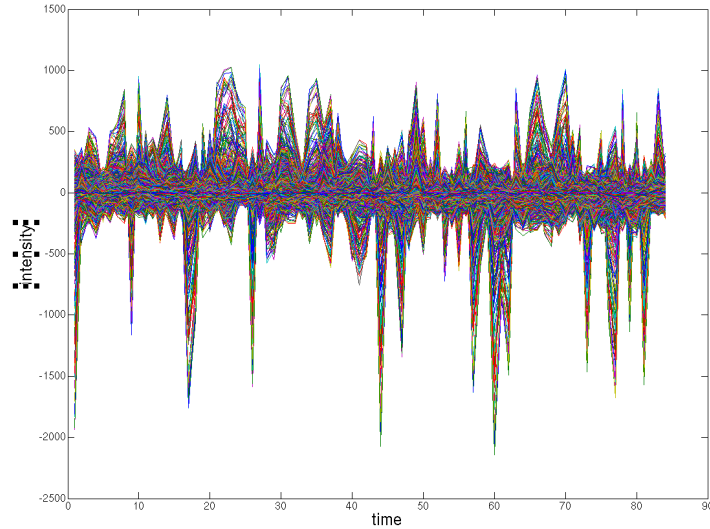


**Fig. 2.** Plots of time series of voxels in axial slice #30 after subtracting their mean values from them. The time series are collapsed in the neighborhood of zero.

The application of the EIHA algorithm with  $\alpha = 20$  to the lattice normalized time series of the whole 3D volume produces the collection of eleven endmembers shown in figure 3. Attending to the intensity scale it can be assumed that the first endmember (top left plot) corresponds to the non activation pattern, while the remaining endmembers correspond to some kind of activation pattern. These patterns correspond to individual voxels and do not reflect aggregated spatial behaviors like in other approaches.

The unmixing process applied to the whole volume voxels with the eleven endmembers of figure 3 produces the abundance images that we interpret as the activation levels of each pattern. To give an interpretation of these activation levels, we refer to the standard results obtained with the SPM software, presented in figure 4 as localized in the Talairach space, in sagittal, coronal and axial cuts. There it can be observed that the activation appears around the axial slice #30. For this reason we present the abundances computed on this slice in figure 5. The figure presents the original slice where the voxels with abundance value above the 99% percentile of the distribution of this endmember abundance over the whole volume are set to white. It can be appreciated that the abundances for endmembers #8 and #11 have some activation regions overlapping the standard detections in figure 4, as well as showing some spurious activation regions. For a complete review of the activation detected by the endmember #11 abundances we show the 99% percentile detection on all the slices in the axial direction in figure 6. The figure shows that there are many spurious detections in slices corresponding to brain regions far away from the activations shown in figure 4.

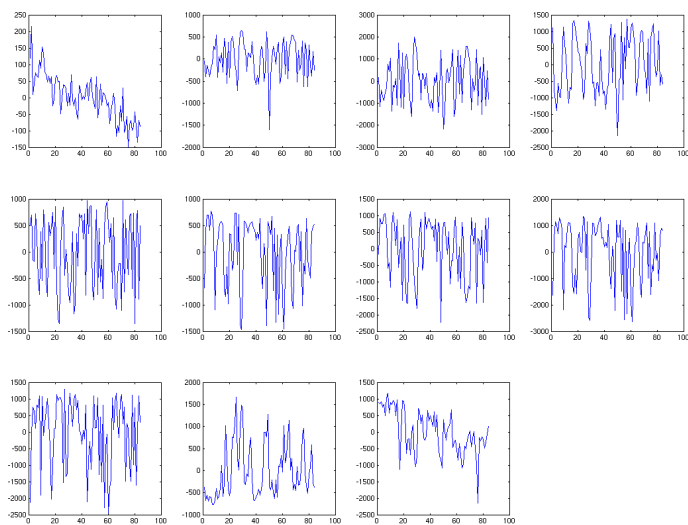


**Fig. 3.** Eleven endmembers detected by EIHA over the lattice normalized time series of the whole 3D volume.

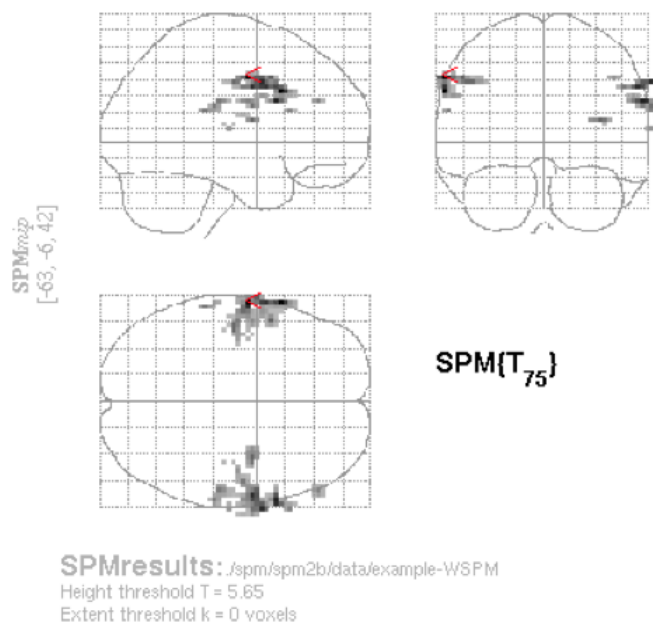


**Fig. 4.** Activation maps from SPM results over the experimental data

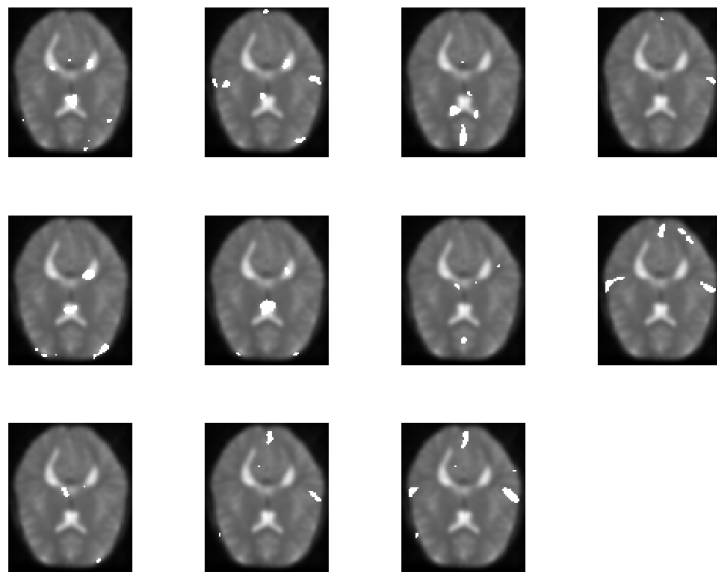


**Fig. 5.** Abundances for axial slice #30 for all eleven endmembers. White voxels correspond to abundance values above the 99% percentile of the distribution of the abundances for each endmember at this slice.

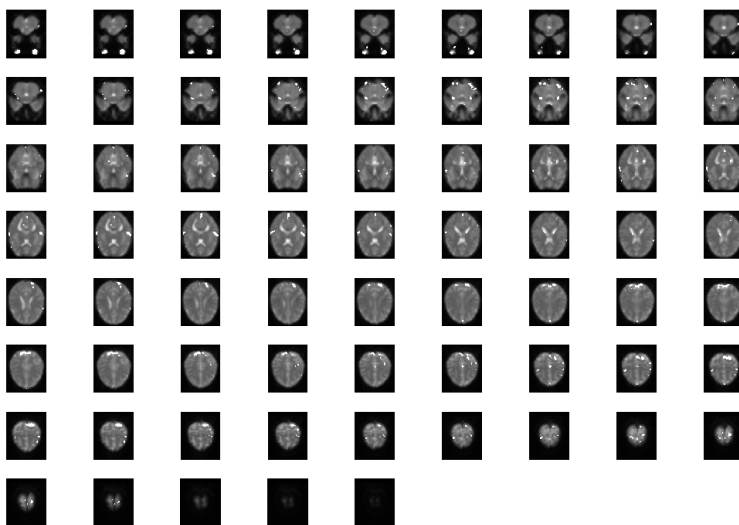


**Fig. 6.** Activations detected by the 99% percentile of the abundance images of endmember #11 of figure 5 in the axial direction.

## 6 Conclusions and Discussion

We have proposed and applied the endmember induction algorithm EIHA discussed in [3] to the task of brain region activation in fMRI. The idea is to try to mimic ICA application to fMRI activation detection [1,13], where the sources correspond to endmembers detected by the EIHA algorithm and the activation is computed as the abundance images obtained by unmixing the voxel time series on the basis of the found endmembers. The first obstacle that we find in this endeavor is that the distribution of the time series is not well aspected for the detection of Lattice Independence as a meaningful characteristic. In fact the voxel's fMRI time series show a dense distribution of intensity displacements from the origin, so almost all of them are lattice dependent and our proposed algorithm only recovers two endmembers. To overcome this problem we propose a normalization which corresponds to a scale normalization in the sense of Lattice Computing. We subtract its mean to each voxel time series. The resulting lattice normalized data set shows a much more rich structure in terms of Lattice Independence. Our computational experiment with a well known fMRI data set, provided with the distribution of the SPM software, show some promising results in the sense that we are able to partially detect activations as the standard analysis with the SPM software. There are however some false detections that show that our approach is not consistent with the SPM analysis. We think that further research may lead to obtain consistent results. One important aspect of SPM is its process of the individual voxel t-test as a random field, this processing is lacking in our initial works. Finding ways to harmonize global random field analysis and our lattice computing approach may lead to such consistency.

## References

1. Calhoun, V.D., Adali, T.: Unmixing fMRI with independent component analysis, *Engineering in Medicine and Biology Magazine, IEEE* (2006) 25(2):79-90
2. Friston, K.J., Holmes, A.P., Worsley, K.J., Poline, J.P., Frith, C.D., Frackowiak, R.S.J.: Statistical parametric maps in functional imaging: A general linear approach, *Hum. Brain Map.* (1995) 2(4):189-210
3. Graña, M., Villaverde, I., Maldonado, J.O., Hernandez, C.: Two Lattice Computing approaches for the unsupervised segmentation of Hyperspectral Images, *Neurocomputing* (2008) in press.
4. Graña, M.: A Brief Review of Lattice Computing, *Proc. WCCI 2008*, pp. 1777-1781
5. Muller, H.-P., Kraft, E., Ludolph, A., Erne, S.N.: New methods in fMRI analysis, *Engineering in Medicine and Biology Magazine, IEEE*, (2002) 21(5):134-142
6. Pekar, J.J.: A brief introduction to functional MRI, *Engineering in Medicine and Biology Magazine, IEEE* (2006) 25(2):24-26
7. Raducanu, B., Graña, M., Albizuri, X.: Morphological scale spaces and associative morphological memories: results on robustness and practical applications, *J. Math. Imaging and Vision* (2003) 19(2):113-122
8. Ritter, G. X., Sussner, P., Diaz-de-Leon, J. L.: Morphological associative memories. *IEEE Trans. on Neural Networks*, (1998) 9(2):281-292,
9. Ritter, G. X., Diaz-de-Leon, J. L., Sussner, P.: Morphological bidirectional associative memories. *Neural Networks*, (1999) 12:851-867,

10. Ritter, G.X., Urcid, G., Iancu, L.: Reconstruction of patterns from noisy inputs using morphological associative memories, *J. Math. Imaging and Vision* (2003) 19(2):95–112
11. Ritter, G.X., Gader, P., Fixed points of lattice transforms and lattice associative memories In: Hawkes P (ed.) *Advances in Imaging and Electron Physics* (2006) 144:165–242, Elsevier, San Diego, CA
12. Ritter, G.X., Urcid, G., Schmalz, M.S.: Autonomous single-pass endmember approximation using lattice auto-associative memories *Neurocomputing* (2008) in press
13. Sarty, G.E.: *Computing Brain Activation Maps from fMRI Time-Series Images*, Cambridge University Press, 2007
14. Strother, S.C., Evaluating fMRI preprocessing pipelines, *Engineering in Medicine and Biology Magazine, IEEE* (2006) 25(2):27-41